2019 EAGE ANNUAL
81ST CONFERENCE + EXHIBITION
LONDON | THE UNITED KINGDOM

WS01_01

A Brief Overview on Seismic Attenuation

J.M. Carcione[1]*

[1] OGS

Summary

Seismic waves decay due to geometrical spreading (in 2D and 3D) and scattering (energy is conserved), and anelastic -- or intrinsic -- attenuation (energy is lost to heat). Amplitude decay in the last two cases is accompanied with wave-velocity dispersion, by which each Fourier component of the signal travels with a different phase velocity (Kramers-Kronig relations). Attenuation can be described by a phenomenological (non-predictive) theory, as the Burgers mechanical model -- composed of springs and dashpots --, or with predictive models, such as the scattering theory, and the Biot and related models of poroelasticity (wave-induced fluid-flow attenuation). Another phenomenological approach is the use of temporal or spatial fractional derivatives, e.g., Kjartansson and Cole-Cole models. In the following, I present a brief overview on the various attenuation mechanisms, where most of the material refers to Carcione (2014).

Introduction

Seismic waves decay due to geometrical spreading (in 2D and 3D) and scattering (energy is conserved), and anelastic – or intrinsic – attenuation (energy is lost to heat). Amplitude decay in the last two cases is accompanied with wave-velocity dispersion, by which each Fourier component of the signal travels with a different phase velocity (Kramers-Kronig relations). Attenuation can be described by a phenomenological (non-predictive) theory, as the Burgers mechanical model – composed of springs and dashpots –, or with predictive models, such as the scattering theory, and the Biot and related models of poroelasticity (wave-induced fluid-flow attenuation). Another phenomenological approach is the use of temporal or spatial fractional derivatives, e.g., Kjartansson and Cole-Cole models. In the following, I present a brief overview on the various attenuation mechanisms, where most of the material refers to Carcione (2014).

Phenomenological models

Mechanical models

The Burgers mechanical model, depicted in Figure 1, describes all the useful models of viscoelasticity, composed of springs and dashpots, whose stress (σ)-strain(ϵ) relations are $\sigma = K\epsilon$ and $\sigma = \eta\dot{\epsilon}$, respectively, where K is stiffness and η is viscosity. The dot above the strain (a time derivative) makes the difference between full energy storage at the spring (no dot), and full dissipation at the dashpot. The concepts can be explained in 1D, considering the Fourier components of the signal, namely a traveling plane wave $\exp[\mathrm{i}(\omega t - kx)]$, where $\mathrm{i} = \sqrt{-1}$, ω is the angular frequency, t is time, k is the complex wavenumber and x is the traveled distance. The complex velocity is $v = \omega/k$, where $k = \kappa - \mathrm{i}\alpha$, with κ the real – physical – wavenumber and α the attenuation factor. It is clear that this plane wave has a phase $\exp[\mathrm{i}(\omega t - \kappa x)]$ and a decay $\exp(-\alpha x)$. The phase velocity and attenuation factor are then

$$v_\mathrm{p} = \frac{\omega}{\kappa} = [\mathrm{Re}(v^{-1})]^{-1} \quad \text{and} \quad \alpha = -\omega \mathrm{Im}(v^{-1}), \tag{1}$$

respectively. Attenuation is usually described with the quality factor, Q, twice the stored energy divided by the dissipated energy, whose expression is

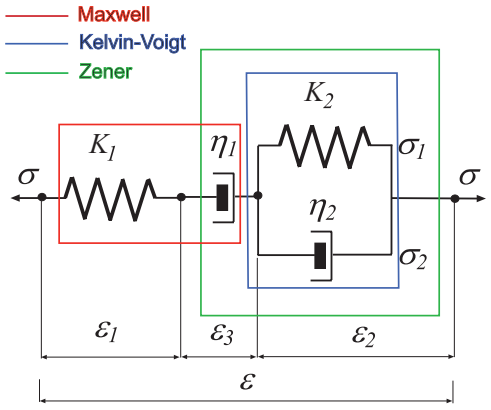

Figure 1 *Burgers viscoelastic model and particular cases.*

$$Q = \frac{\mathrm{Re}(v^2)}{\mathrm{Im}(v^2)}, \quad \text{with } \alpha/\kappa = \sqrt{1+Q^2} - Q, \quad \alpha = \frac{\omega}{Q v_\mathrm{p}} \ (Q \gg 1) \tag{2}$$

(Carcione, 2014). Typical values of reservoir-rock P and S seismic Q factors are in the range 10–100. These expressions hold also in 2D and 3D for each wave type (P and the two S) and homogeneous waves, i.e., when the real wavevector points in the same direction as the attenuation vector. As an example, consider the Kelvin-Voigt model (see Figure 1). In the Fourier domain, $\sigma_1 = K_2\epsilon_2$ and $\sigma_2 = \mathrm{i}\omega\eta_2\epsilon_2$, where σ_1 and σ_2 are the stresses acting on the spring and dashpot, respectively. Since $\sigma = \sigma_1 + \sigma_2$, the stress-strain relation is $\sigma = (K_2 + \mathrm{i}\omega\eta_2)\epsilon_2 \equiv M\epsilon_2$, the complex velocity is $v = \sqrt{M/\rho}$, (ρ is the mass density), and $Q = K_2/(\omega\eta_2)$. Removing the dashpot (η_2 = 0) gives a lossless medium, i.e., an infinite Q factor. The Kelvin-Voigt model describes a solid with wave loss, but rocks (and metals) are better described with the Zener model (Zener, 1948), which has a relaxation peak in Q^{-1} as a function of frequency, and whose phase velocity is bounded between a lower limit (at ω = 0) and an upper limit (at $\omega = \infty$).

The energy velocity is defined as the ratio of the average energy flux to the average total energy density. It equals the phase velocity in isotropic media. In 3D anisotropic and viscoelastic media, $\boldsymbol{\sigma} = \mathbf{C} \cdot \boldsymbol{\epsilon}$, a scalar product of a 6×6 complex (and frequency dependent) stiffness matrix, $\mathbf{C}$, with a six-components

array $\boldsymbol{\epsilon}$ (in the so-called Voigt notation). In 3D pore-viscoelasticity, $\mathbf{C}$ is a 7×7 matrix, and equations (1) and (2) equally hold, with these properties being direction dependent. The reciprocal of the phase velocity (slowness surface) describes the propagation of plane waves. The group and energy velocity describe the location of the wavefront, and are equal only in the elastic limits. At finite frequencies, the group velocity looses its physical meaning, and as a kinematic concept can be replaced with the envelope velocity, which is a good approximation of the energy velocity (Carcione, 2014). To be more rigorous, the concept of centrovelocity is introduced in Carcione at el. (2010a), related to the centroid of the pulse in the time and spatial domains.

The analysis can also be performed for standing waves, $\exp[\mathrm{i}(\Omega t - \kappa x)] = \exp[\mathrm{i}(\omega t - \kappa x)]\exp(-\omega_I t)$, where $\Omega = \omega + \mathrm{i}\omega_I$ is complex. In this case, $v = \Omega/\kappa$, $v_\mathrm{p} = \mathrm{Re}(v)$, $\omega_I = (\omega/v_\mathrm{p})\mathrm{Im}(v)$, and the energy velocity and Q factor have the expression (1) and (2), respectively.

Fractional-derivative models

Attenuation can also be modeled with fractional derivatives (e.g., Picotti and Carcione, 2017). An example is the fractional Kelvin-Voigt model, where the time derivative of the strain in the dashpot (the dot) is replaced by ∂_t^q, where q is the order of the derivative. Then, $\sigma = K\epsilon + \eta\partial_t^q$, $0 \le q \le 1$, where η is a pseudo-viscosity, which is a stiffness for q = 0 and a viscosity for q = 1. The limits $q = 0$ and $q = 1$ give Hooke's law and the constitutive relation of the Kelvin-Voigt model, respectively. In the frequency domain, $M = K + \eta(\mathrm{i}\omega)^q$. If K = 0, we obtain a constant $Q = \cot(\pi q/2)$, as in Kjartansson (1979). Simulations with fractional time derivatives require much memory storage. On the other hand, fractional spatial derivates are more efficient. For instance, the uniform-density pressure (p) wave equation is $\omega_0^{2-q} c^q \partial_x^q p = \partial_t^2 p$, where ω_0 is a reference frequency and $2 \le q \le 4$ (q = 2 yields the classical wave equation). In the Fourier domain, $\partial_x^q \to (\mathrm{i}k)^q$, $v = c(\mathrm{i}\omega/\omega_0)^{1-2/q}$ (Kjartansson, 1979) and $Q = -\cot(2\pi/q)$ is constant with frequency. In both cases (time and spatial fractional derivatives), q = 2 gives the lossless case, i.e., $Q = \infty$. Attenuation is a low-pass filter, since the decay factor is approximately $\exp(-\omega x/\beta)$, where $\beta = 2Qv_\mathrm{p} \approx$ constant, for a frequency-independent Q factor.

Predictive models

Scattering occurs as reflection, refraction, and diffraction of elastic energy, and this is conserved. A major cause of attenuation in porous media, at the reservoir scale, is wave-induced fluid flow, which occurs at different spatial scales. The flow can be classified as macroscopic, microscopic and mesoscopic. At larger scales, grain boundary relaxation is the predominant cause of seismic attenuation in the Earth's crust and mantle.

Scattering

At low frequencies, when the wavelength is much larger than the characteristic scales of heterogeneity, the medium behaves like an equivalent medium, e.g., finely-layered media is a transversely isotropic homogeneous medium (Backus averaging is its mathematical model). At high frequencies, scattering attenuation causes energy to be distributed into coda waves and the primary pulse behaves viscoelastic of the Zener type (e.g., Kikuchi, 1981). Intrinsic (α_i) and scattering (α_s) attenuations are approximately additive, since the decay factor is $\exp(-\alpha_i x)\exp(-\alpha_s x) = \exp[-(\alpha_i + \alpha_s)x]$, and in the low-loss case ($Q \gg 1$), the total dissipation factor is

$$Q^{-1} = Q_i^{-1} + Q_s^{-1}, \tag{3}$$

based on equation (2). Both types of attenuation can, in principle, be separated on the basis of equation (3) and a proper scattering theory (Frankel and Wennerberg, 1987). The location of the scattering peak is inversely proportional to the size of the heterogeneity. For instance, for cracks of length a the peak P-wave loss frequency is

$$f_s \approx \frac{v_\mathrm{P}}{5a}, \tag{4}$$

where v_P is the P-wave velocity (Kikuchi, 1981).

Wave-induced fluid-flow attenuation

Macroscopic Biot attenuation: The attenuation mechanism predicted by Biot in 1956 has a macroscopic nature. It is the wavelength-scale equilibration between the peaks and troughs of the P wave. The dissipation factor of the fast P wave, Q^{-1}, can be approximated by that of a Zener model. The location of the relaxation peak is

$$f_B \approx \frac{\phi\eta\rho}{2\pi\bar{\kappa}\rho_f(\rho\mathcal{T}-\phi\rho_f)}, \tag{5}$$

where ϕ is the porosity, η is the fluid viscosity, ρ is the bulk density, $\bar{\kappa}$ is the permeability, ρ_f is the fluid density, and $\mathcal{T}$ is the rock tortuosity. This equation shows that the relaxation peak moves towards the high frequencies with increasing viscosity and decreasing permeability. This means that, at low frequencies, attenuation decreases with increasing viscosity (or decreasing permeability). This is in contradiction with experimental data at seismic and sonic frequencies, since the macroscopic-flow mechanism underestimates the wave-velocity dispersion and attenuation in rocks.

Microscopic squirt-flow attenuation: An important attenuation mechanism in rocks is the the so-called "squirt flow", by which there is flow from fluid-filled micro-cracks (or grain contacts) to the pore space and back. Biot (1962) considered this mechanism and proposed the Zener mechanical model to describe it. The squirt-flow model assumes that the rock becomes stiffer when the fluid pressure does not have enough time to equilibrate between the stiff and compliant pores (grain contacts and main voids, respectively). This state is described by the unrelaxed limit of Zener elements. The squirt-flow peak frequency is

$$f_{sf} \approx \frac{K_s r^2}{3\pi\eta\gamma}, \quad \gamma = \frac{K_s}{\phi_c}\left(\frac{1}{K_m}-\frac{1}{K_h}\right), \tag{6}$$

where r is the crack thickness to crack length ratio, ϕ_c is the compliant porosity and K_h is the dry-rock bulk modulus at a confining pressure when all the compliant pores are closed, i.e., an hypothetical rock without the soft porosity (Carcione and Gurevich, 2011).

Mesoscopic attenuation: Local fluid flow explains the high attenuation of low-frequency waves in fluid-saturated rocks. When seismic waves propagate through small-scale heterogeneities, pressure gradients are induced between regions of dissimilar properties. White (1975) was the first to show that attenuation and velocity dispersion measurements can be explained by the combined effect of mesoscopic-scale inhomogeneities and energy transfer between wave modes, with P-wave to slow P (Biot)-wave conversion being the main physical mechanism. I refer to this mechanism as mesoscopic loss. The mesoscopic-scale length is intended to be larger than the grain sizes but much smaller than the wavelength of the pulse. A review of the different theories and authors, who have contributed to the understanding of this mechanism, can be found in Müller et al. (2010), Carcione et al. (2010b) and Carcione (2014). At seismic frequencies, the mesoscopic loss mechanism seems to be dominant. Mesoscopic patches of gas in a water saturated sandstone dissipate significant energy through conversion to the diffusive slow mode. The corresponding peak frequency is

$$f_m \approx \frac{\bar{\kappa}K_f}{\phi\eta a^2}, \tag{7}$$

where here a is the size of the patches and K_f is fluid bulk modulus. Note the inverse dependence on $\bar{\kappa}/\eta$ compared to the Biot mechanism in equation (5). Generalization of the Biot theory to the case of multiple material phases and/or double porosity describe more realistic situations (see Ba et al., 2015).

Ductility and partial melting. Grain boundary relaxation

Seismic propagation in the upper part of the crust, where geothermal reservoirs are located, shows strong velocity dispersion and attenuation due to varying permeability and saturation conditions and is affected by the brittle-ductile transition (BDT), including zones of partial melting. From the elastic-plastic aspect, the seismic properties (velocity, quality factor and density) depend on effective pressure and temperature. The related effects can be described with the Burgers mechanical model applied to the shear modulus of the dry rock. The Arrhenius equation combined with the octahedral stress criterion define the Burgers

viscosity responsible of the ductile behaviour of partial melting through a process called grain boundary relaxation (Carcione et al., 2018). The viscosity of the earth highly affects the S waves to the point that they disappear at total melting. P waves show high attenuation and dispersion (Zener-like peaks) with frequency and temperature – at a critical temperature, which depends on frequency and the Burgers viscosity. Seismic-wave behaviour in the presence of partial melt can be used to identify the BDT.

Conclusions (*peak frequencies for a sandstone*)

Consider the material properties for a water-saturated sandstone (see table). Using Gassmann equations (e.g., Carcione, 2014), the P-wave velocity is $v_{\rm P}$ = 3366 m/s, and the bulk density is ρ = 2167 kg/m^3. Assuming a = 10 cm and r = 0.0008, the relaxation frequencies of the different attenuation mechanisms are: f_s = 6.7 kHz (scattering), f_B = 213 kHz (Biot global flow), f_{sf} = 815 Hz (squirt flow, with ϕ_c = 0.0002, K_h = 12 GPa), and f_m = 75 Hz (mesoscopic). While scattering has a peak at the sonic frequencies and the Biot one is dominant at high (laboratory) frequencies, the squirt-flow and mesoscopic loss mechanisms are important at VSP and seismic frequencies. Replacing water by oil (ρ_f = 800 kg/m^3, K_f = 2 GPa and η = 100 cP), the peak frequencies are f_s = 6.8 kHz, f_B = 27 MHz, f_{sf} = 8 Hz, and f_m = 0.7 Hz.

Grain	Bulk modulus, K_s	40.	GPa
	Density, ρ_s	2650	kg/m^3
Matrix	Porosity, ϕ	0.3	
	Bulk modulus, K_m	10	GPa
	Shear modulus, μ_m	8	GPa
	Permeability, $\bar{\kappa}$	100	mD
	Tortuosity, $\mathcal{T}$	2.3	
Fluid	Bulk modulus, K_f	2.25	GPa
	Density, ρ_f	1040	kg/m^3
	Viscosity, η	1	cP

References

Ba, J., Carcione, J. M., Du, O., Zhao, H., and Müller, T. M., 2015, Seismic exploration of hydrocarbons in heterogeneous reservoirs: New theories, methods and applications, Elsevier Science.

Biot, M. A., 1962, Mechanics of deformation and acoustic propagation in porous media, J. Appl. Phys., 33, 1482–1498.

Carcione, J. M., 2014, Wave Fields in Real Media. Theory and numerical simulation of wave propagation in anisotropic, anelastic, porous and electromagnetic media, Elsevier. (Third edition, extended and revised).

Carcione, J. M., Gei, D., and Treitel, S., 2010a, The velocity of energy through a dissipative medium, Geophysics, 75, T37–T47.

Carcione, J. M., and Gurevich, B., 2011, Differential form and numerical implementation of Biot's poroelasticity equations with squirt dissipation, Geophysics, 76, N55–N64.

Carcione, J. M., Poletto, F., Farina, B., and Bellezza, C., 2018, 3D seismic modeling in geothermal reservoirs with a distribution of steam patch sizes, permeabilities and saturations, including ductility of the rock frame, Phys. Earth Planet. Inter., 279, 67–78.

Frankel, A., and Wennerberg, L., 1987, Energy-flux model of seismic coda: separation of scattering and intrinsic attenuation, Bull. Seism. Soc. Am., 77(4), 1223–1251.

Kikuchi, M., 1981, Dispersion and attenuation of elastic waves due to multiple scattering from cracks, Phys. Earth Planet. Inter., 27, 10–105.

Kjartansson, E., 1979, Constant Q wave propagation and attenuation, J. Geophys. Res., 84, 4737–4748.

Müller, T. M., Gurevich, G., and Lebedev, M., 2010, Seismic wave attenuation and dispersion resulting from wave-induced flow in porous rocks – A review, Geophysics, 75(5), 75A147–75A164.

Picotti, S. and Carcione, J. M., 2017, Numerical simulation of wave-induced fluid flow seismic attenuation based on the Cole-Cole model, J. Acous. Soc. Am., 142, 134; http://dx.doi.org/10.1121/1.4990965.

White, J. E., 1975, Computed seismic speeds and attenuation in rocks with partial gas saturation, Geophysics, 40, 224–232.

Zener, C., 1948, Elasticity and anelasticity of metals. University of Chicago Press.